

Fröhlich Condensation of Bosons: Graph texture of curl flux network for nonequilibrium properties

Feihong Liu,¹ Chase Slowey,² Xuanhua Wang,³ Dangyuan Lei,^{1,4} Zhiyue Lu,^{2,*} and Zhedong Zhang^{4,5,†}

¹*Department of Materials Science & Engineering,*

City University of Hong Kong, Kowloon, Hong Kong SAR

²*Department of Chemistry, University of North Carolina at Chapel Hill,*

Chapel Hill, North Carolina 27599, United States

³*Center for Theoretical Interdisciplinary Sciences, Wenzhou Institute,*

University of Chinese Academy of Sciences, Wenzhou, Zhejiang 325001, China

⁴*Department of Physics, City University of Hong Kong, Kowloon, Hong Kong SAR*

⁵*Shenzhen Research Institute, City University of Hong Kong, Shenzhen, Guangdong 518057, China*

(Dated: June 3, 2025)

Nonequilibrium condensates of bosons subject to energy pump and dissipation are investigated, manifesting the Fröhlich coherence proposed in 1968. A quantum theory is developed to capture such a nonequilibrium nature, yielding a certain graphic structure arising from the detailed-balance breaking. The results show a network of probability curl fluxes that reveals a graph topology. The winding number associated with the flux network is thus identified as a new order parameter for the phase transition towards the Fröhlich condensation (FC), not attainable by the symmetry breaking. Our work demonstrates a global property of the FCs, in significant conjunction with the coherence of cavity polaritons that may exhibit robust cooperative phases driven far from equilibrium.

Introduction.—Nonequilibrium condensates have drawn broad attention in a variety of systems during past decades, including proteins, organic molecules, magnetic materials, polymers, etc. [1–7]. As a prominent member of the nonequilibrium condensates, Fröhlich condensation exhibits a cooperative phase that incredibly emerges alongside the energy dissipation [8–11]. An external energy pump and dissipation act on the molecules, essentially driving to the far-from-equilibrium regime whereby the energy redistribution as a typical nonlinear feature plays a pivotal role. Such a paradigm leads to a nonequilibrium phase transition, laying the foundation for a unified understanding of various newly-emerging phases reported recently [12–17].

So far, the nonequilibrium condensations of bosons have been observed in complex systems including phonons, polaritons, polymers, etc. [8, 18–22]. A notable regime is the so-called Fröhlich condensate which was proposed originally for protein vibrations driven far from equilibrium [8, 23]. In the presence of strong energy pump, the dissipation and energy redistribution do interplay with each other, yielding a critical pumping power for achieving a large accumulation of bosons at the lowest mode. In such a vein, Nardecchia, et al. observed the phonon condensation phase in model proteins using the THz spectroscopic technique [24]. The exciton-polariton condensation was observed in semiconductor quantum wells and monolayer perovskites, demonstrating the long-range coherence and ultrafast switch that enable a versatile use of information processing [20, 25–28]. Despite these remarkable achievements, the microscopic origin of the nonequilibrium condensations is still an open issue. Notably, for the polariton condensates, an intense debate on the underlying mechanism—whether the

condensation phase resides in a different category—has been lasted for decades [29–35]. The driven-dissipative nature was shown to reveal unusual fluctuations of polaritons [36, 37]. This may indicate the far-from-equilibrium regime, resembling the Fröhlich coherence. Nevertheless, a full counting statistics deviating from the equilibrium states still lacks, although several indications were actively discussed before [29, 38–43]. Moreover, the thermodynamic irreversibility arising from the nonequilibrium nature led to an inevitable ambiguity of describing the Fröhlich condensates, once being aware of the U(1) symmetry breaking.

In this Letter, we present a full quantum theory for the nonequilibrium condensates of bosons that may possess a graphic structure, beyond the scope of the symmetry-breaking paradigm. Our results reveal a strong correlation between the condensates and the total particle number, which essentially breaks the detailed balance. A probability flux network emerges, forming 2D graphs associated with certain topology. We elaborate on the curl nature of the flux network and find out the winding number that is a topological invariant as a new order parameter for such nonequilibrium phase transition. Our work demonstrates the Fröhlich coherence in a broader context of driven-dissipative systems, e.g., polaritons. A new class of nonequilibrium matter can be therefore expected.

Driven-dissipative model of phonons.—The vibrations in molecules, e.g., vibrations of J/H aggregates and DNA backbones, are surrounded by dense mediums (like solvent or water) that act as a thermal environment. This results in the channels of energy dissipation and internal conversion (IC). The latter is responsible for the energy redistribution amongst the vibrations, thus generating

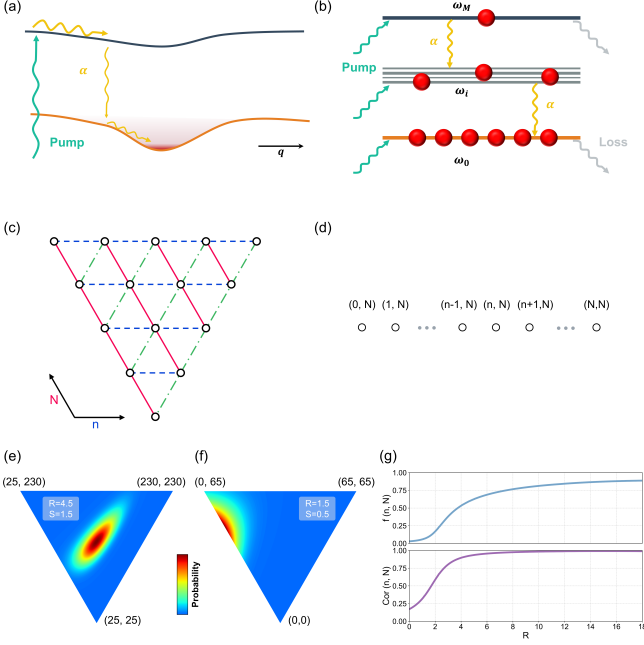


FIG. 1. (a) Schematic illustration of phonon dispersion and relaxation towards the lowest-energy mode. (b) Level structure for bosons subject to external energy pump and dissipation. (c) 2D hexagonal-grid graph for nonequilibrium bosons mapped from Eq.(2). (d) Graph for the BEC phase where all the sites are disconnected. (e) Steady-state number distribution $P_{n,N}$ when pump is above the threshold; (f) $P_{n,N}$ when pump is below the threshold. (g, up) Condensation fraction f against pump rate [$R = 3S$]; (g, down) Pearson correlation between n and N against pump rate [$R = 3S$].

the nonlinearity. Besides, the vibrations are driven by an external energy pump.

For a neat picture, we adopt the phonon model with a sandwich structure of energy levels that contains $M + 1$ modes depicted in Fig.1(a). The lowest mode has the energy ω_0 , whereby the excited modes are densely distributing that yields a high density of states. The free Hamiltonian is $H_0 = \sum_{i=0}^M \omega_i \eta_i^\dagger \eta_i$; $\omega_1, \omega_2, \dots, \omega_M$ denote the energies of excited modes that are normally presented in a narrow bandwidth. η_i and η_i^\dagger are the respective bosonic annihilation and creation operators, i.e., $[\eta_i, \eta_j^\dagger] = \delta_{ij}$. With the effects of external pump and environment, the interaction reads

$$V(t) = \sum_i \eta_i F_i(t) e^{-i\omega_i t} + \sum_{i \neq j} \beta_{ij} \eta_i^\dagger \eta_j q(t) e^{i(\omega_i - \omega_j)t} + \text{h.c.} \quad (1)$$

where $F_i(t)$ is the energy pump with $\langle F_i(t) F_j(t') \rangle = r_i \delta_{ij} \delta(t - t')$ that is broadband. $q(t)$ is the dimensionless coordinate of the environment described by a group of harmonic oscillators.

The parameter β_{ij} measuring the IC rate in Eq.(1) can be computed from sophisticated models [44].

Reduced dynamics of the ω_0 mode.—Defining the re-

duced density matrix for the ω_0 mode, $\sigma_{n,N;n+\Delta,N+\Delta} = \sum'_{\{n_k\}} \langle n; \{n_k\} | \rho | n + \Delta; \{n_k\} \rangle$ with N being the total particle number and $\{n_k\} \equiv n_1, \dots, n_M$ where the $\sum'_{\{n_k\}}$ is subject to $n + n_1 + \dots + n_M = N$, the equation of motion (EOM) can be derived. We proceed via the dynamical equation

$$\dot{\sigma}_{n,N;n',N'} = - \sum_i \sum'_{\{n_k\}} \int_{t_i}^t dt' \langle n, \{n_k\} | \text{Tr}_E [V(t - t_i), \times [V(t' - t_i), \rho(t')]] | n', \{n_k\} \rangle$$

where Tr_E denotes the average over the solvent environments and the summation excludes the ω_0 mode.

Using the results above, one finds the EOM for the ω_0 mode ($P_{n,N} \equiv \sigma_{n,N;n,N}$) [44, 45]

$$\begin{aligned} \dot{P}_{n,N} = & + n [R P_{n-1,N-1} - (R+1) P_{n,N}] \\ & - (n+1) [R P_{n,N} - (R+1) P_{n+1,N+1}] \\ & + [S \mathcal{A}_{n,N-1} P_{n,N-1} - (S+1) \mathcal{B}_{n,N} P_{n,N}] \\ & - [S \mathcal{A}_{n,N} P_{n,N} - (S+1) \mathcal{B}_{n,N+1} P_{n,N+1}] \\ & + \alpha n [\mathcal{K}_{n-1,N} P_{n-1,N} - \mathcal{H}_{n,N} P_{n,N}] \\ & - \alpha (n+1) [\mathcal{K}_{n,N} P_{n,N} - \mathcal{H}_{n+1,N} P_{n+1,N}] \end{aligned} \quad (2)$$

with $\mathcal{A}_{n,N} = \sum_{j=1}^M \langle n_j + 1 \rangle_{n,N}$, $\mathcal{B}_{n,N} = \sum_{j=1}^M \langle n_j \rangle_{n,N}$, $\mathcal{K}_{n,N} = \sum_{j=1}^M (\bar{n}_{j0} + 1) \langle n_j \rangle_{n,N}$, and $\mathcal{H}_{n,N} = \sum_{j=1}^M \bar{n}_{j0} \langle n_j + 1 \rangle_{n,N}$, where $\langle \dots \rangle_{n,N}$ denotes the mean, given n, N . $R = r_0/\gamma$, $S = r_j/\gamma$, $\alpha = 2\pi |\beta_\omega \lambda_\omega|^2 \mathcal{D}(\omega)/\gamma$ are the respective rates of energy pump at ω_0 mode, the j th state, and the nonradiative transition rate between the phonon modes; all have been rescaled by the radiative decay rate γ . $\bar{n}_{j0} = [e^{(\omega_j - \omega_0)/T} - 1]^{-1}$ is a Planck factor. There are varying degrees of rigor to evaluate $\mathcal{A}_{n,N}$, $\mathcal{B}_{n,N}$, $\mathcal{K}_{n,N}$, $\mathcal{H}_{n,N}$. We choose the one such that $\bar{n}_{j0} \approx \bar{n}$ which gives $\mathcal{A}_{n,N} = N + M - n$, $\mathcal{B}_{n,N} = N - n$, $\mathcal{K}_{n,N} = (\bar{n} + 1)(N - n)$, $\mathcal{H}_{n,N} = \bar{n}(N + M - n)$.

Elaborate illustration in Fig.1(c) depicts Eq.(2) in terms of a probability current network. This will be elaborated later on.

Eq.(2) can be recast into the form $\dot{P} = WP$ in Liouville space, where the vector $P = (P_{0,0}, P_{0,1}, \dots, P_{n,N}, \dots)^T$ and W is a square matrix. $W_{n',N';n,N} P_{n,N}$ accounts for the rate of forward transition $(n, N) \rightarrow (n', N')$, and then the rate of backward transition $(n', N') \rightarrow (n, N)$ follows, i.e., $W_{n,N;n',N'} P_{n',N'}$. These two transition rates cannot be equal normally, and therefore elucidates the detailed-balance breaking.

Nonequilibrium condensation of bosons.—From Eq.(2) one can find the equations for the means of n and N , i.e., $C = (M+1)\bar{n} + 1 + \alpha^{-1}$ and

$$\langle \dot{n} \rangle = \alpha \langle (N - C)n \rangle - \alpha \langle n^2 \rangle + \alpha (\bar{n} + 1) \langle N \rangle + R \quad (3a)$$

$$\langle \dot{N} \rangle = R + MS - \langle N \rangle. \quad (3b)$$

Eqs.(3a,3b) evidence a pump threshold R_c, S_c , above which an inflation occurs—a condensation at ω_0 . For a back-of-the-envelope understanding, one can presumably neglect the fluctuation of N , i.e., $\langle nN \rangle \approx \langle n \rangle N$ [19, 39]. This gives an estimation $R_c + MS_c = C$.

The condensation transition is calculated in an explicit way, i.e., the fraction $f = \frac{\langle n \rangle}{\langle N \rangle}$ using Eq.(2), once being aware of drastic fluctuations in the vicinity of critical point. We plot the results in Fig.1(g,up), depicting a sharp increase towards a high f at strong pump.

Nevertheless, one should note that the n, N fluctuations are strongly correlated with each other, when above R_c, S_c . Such an insight underlines the essential of an advanced theory beyond the present understanding.

Curl flux network and detailed balance violation.—Eq.(2) can be solved for the steady-state number distribution $P_{n,N}$, depicted in Fig.1(e,f). With higher pump power, $P_{n,N}$ reveals two insights: (1) a transition from thermal to coherent statistics; (2) a stronger n - N correlation once the condensates are formed [see Fig.1(g,down)]. The nonequilibrium nature is thus inferred, signifying the fluctuation of N .

Eq.(2) is readily mapped to a hexagonal-grid graph via the net edge currents

$$J_{(n,N) \rightarrow (n',N')} = W_{n',N';n,N} P_{n,N} - W_{n,N;n',N'} P_{n',N'} \quad (4)$$

as shown in Fig.1(c). One thus has $W_{n,N;n-1,N-1} = nR$, $W_{n-1,N-1;n,N} = n(R+1)$, etc.. Eq.(2) reads $\dot{P}_{n,N} = J_{(n-1,N-1) \rightarrow (n,N)} - J_{(n,N) \rightarrow (n+1,N+1)} + J_{(n,N-1) \rightarrow (n,N)} - J_{(n,N) \rightarrow (n,N+1)} + J_{(n-1,N) \rightarrow (n,N)} - J_{(n,N) \rightarrow (n+1,N)}$, which forms certain tree connections that give the topology of the graph [46, 47]. The flux network has been extensively studied in classical stochastic processes [48–51]. For quantum systems, the concept of flux network was developed in recent progresses [52–54].

$J_{(n,N) \rightarrow (n',N')} \neq 0$ measures how far the system deviates from the equilibrium, thus breaking the detailed balance. When the condensates emerge, J s on the graph consist of loop currents. To see this closely, we essentially develop two theorems as follows.

Theorem 1. *There exists nonvanishing edge currents for the Fröhlich condensates, i.e., $J_{(n,N) \rightarrow (n',N')} \neq 0$.*

Proof. Suppose $J_{(n,N) \rightarrow (n',N')} = 0$ in Eq.(4). Given $n \leq N$, one can count the number of the elementary arrows in Fig.1(c), which gives independent edge currents. Thus

$$[I + (I-1) + \dots + 1] + [I + (I-1) + \dots + 1] + [I + (I-1) + \dots + 1]$$

which yields $1.5I(I+1)$ independent linear equations for $P_{n,N}$, with $I \rightarrow \infty$. However, the number of independent $P_{n,N}$ is

$$\frac{(I+1)(I+2)}{2} - 1 = \frac{I(I+3)}{2}. \quad (5)$$

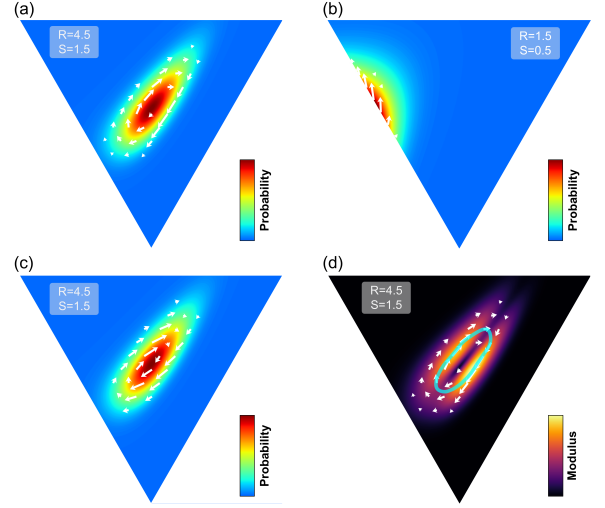


FIG. 2. Curl flux (white arrows) J_c and number distribution for (a) FC phase in the above-threshold regime, (b) thermal phase in the below-threshold regime, where the flux is calculated from Eq.(12). Obviously, no loops are presented in thermal phase. (c) Current network (white arrows) obtained from Eq.(4), showing the curl nature consistent with (a). (d) Modulus $|J_c|$ revealing a Mount-Fuji landscape with a ring valley; green loop on the ridge locates the maximum curl flux.

Then

$$[\# \text{ of equations}] - [\# \text{ of unknowns}] = I^2 \gg 1. \quad (6)$$

The group of linear homogeneous equations for $P_{n,N}$ is overcomplete. This gives rise to $P_{n,N} = 0$ in general. Therefore $J_{(n,N) \rightarrow (n',N')} \neq 0$ for nonvanishing $P_{n,N}$. \square

Theorem 2. *The detailed balance holds with pump off, i.e., $J_{(n,N) \rightarrow (n',N')} = 0$. This gives BEC on a null graph.*

Proof. When the pump is off, the N is fixed. The EOM reduces to $\dot{P}_{n,N} = J_{(n-1,N) \rightarrow (n,N)} - J_{(n,N) \rightarrow (n+1,N)}$. The finite graph arising from $0 \leq n \leq N$, shown in Fig.1(d), requires $J_{(n-1,N) \rightarrow (n,N)} = 0$, yielding

$$[\# \text{ of equations}] = N, \quad [\# \text{ of unknowns}] = N, \quad (7)$$

which solves for unique steady state of BECs [55]. The graph is depicted in Fig.1(d), which is null. \square

Theorems 1 and 2 elucidate the nonequilibrium nature of the FCs, indicating a graph texture readily distinct from the BECs. This may lead to a new order parameter based on graph topology, and will be elaborated.

Off-diagonal long-range order (ODLRO).—The reduced density matrix defined in Eq.(2) is of a standard form for a state with ODLRO. In particular, it has $\text{ODLRO} = \lim_{|m-n| \rightarrow \infty} \langle b_m^\dagger b_n \rangle$ where b_n is the operator for the vibrations at local site. Using η operators, one

can calculate from Eq.(2) that

$$\text{ODLRO} = \frac{\langle n \rangle}{2M} e^{i\mathbf{k} \cdot \mathbf{L}}; \quad |\mathbf{L}| \text{ is sample length.} \quad (8)$$

It is known that the ODLRO is an explicit expression of the global U(1)-symmetry breaking [56–59].

Graph topology and order parameter for condensates.—The analysis can proceed for a clear form of curl fluxes, through the continuous limit, i.e., with a large volume V . Thereby one defines two variables in a hexagonal frame

$$x = \frac{n}{V}, \quad y = \frac{N}{V} \quad (9)$$

such that x, y become continuous as $V \rightarrow \infty$. In a Cartesian frame such that $X = x - \frac{y}{2}$, $Y = \frac{\sqrt{3}y}{2}$, one reforms Eq.(2) into a partial differential equation [44, 60]

$$\partial_t P + \nabla \cdot \mathbf{J} = 0 \quad (10)$$

with the curl flux in the form of

$$\mathbf{J}(X, Y) = \mathbf{F}P - \nabla \cdot (\mathbf{D}P). \quad (11)$$

Eq.(11) may possess nontrivial topology arising from the detail-balance breaking. To see this clearly, we extend \mathbf{J} onto complex domain, i.e., $(X, Y) \rightarrow z \equiv X + iY$

$$J_c(z, z^*) = J_X - iJ_Y. \quad (12)$$

J_c is not entirely analytic, thus $\oint J_c(z, z^*) dz \neq 0$ when enclosing a point z_m . The following theorem is useful.

Theorem 3. $J_c(z_m, z_m^*) = 0$, given the curl fluxes enclosing z_m .

Proof. The proof is straightforward, as given in Ref.[44]. \square

Theorem 3 indicates that J_c is ill-defined at z_m . The curl flux should exhibit a vortex, yielding a topological structure associated with the condensate.

The topological structure of the curl fluxes can be clarified by the homotopy group. J_c reveals a cycling nature when having the condensates—as a result of the divergence free and homogeneous boundaries shown in Fig.2(a)—which forms a U(1) space. This enables a mapping: $U(1) \rightarrow S^1_\phi$ where $S^1_\phi = \phi \in [0, 2\pi]$ is a circle. Such a mapping can be characterized by integer winding numbers, i.e., $e^{in\theta}$, $0 \leq \theta < 2\pi$ [61]. One can denotes this fact symbolically as, in terms of the fundamental group, $\pi_1[U(1)] = \{0, 1, 2, \dots\}$.

In contrast, J_c does not show loops at the below-threshold regime. Instead, a bundle of open lines (denoted by e) are observed, corresponding to the thermal phase. The BEC phase, from Theorem 2, disconnects all the trees, creating a null graph \emptyset . Therefore an exact mapping is established, i.e.,

$$\begin{aligned} \text{FCs} : \pi_1[U(1)] &= \mathbb{Z}; \quad \mathbb{Z} = \{0, 1, 2, \dots\} \\ \text{Thermal} : \pi_1[e] &= 0, \quad \text{BECs} : \pi_1[\emptyset] = 0. \end{aligned} \quad (13)$$

Eq.(13) indicates a graphic order parameter for the condensation transition. To see this closely, one reforms the flux $J_c(z, z^*) = |J_c| \exp(iS)$ so that the phase S may have a pole at z_m . The winding number thus follows, in a form of

$$Q = \frac{1}{2\pi} \oint \partial_{\mathbf{R}} S(\mathbf{R}) \cdot d\mathbf{R} = \frac{1}{4\pi} \int F_{\mu\nu} dR_\mu \wedge dR_\nu \quad (14)$$

where the connection tensor $F_{\mu\nu} = [\partial_\mu, \partial_\nu]S(\mathbf{R})$. Q is thus a topological invariant residing in the group \mathbb{Z} . In our case, $Q = 1$ so that $\pi_1[U(1)] = 1$ resulting from a single-fold circulating shown in Fig.2(a,c).

Table 1 collects the symmetry and graph topology for the three different phases. Notably, the polariton condensation (PC) as a promising driven-dissipative system obeys the EOM sharing the structure of Eq.(2) [39, 62]. The PC thus resides in the FC regime, exhibiting a graph texture distinct from the BEC phase.

Fig.2 shows the 2D curl fluxes given by Eq.(12). From Fig.2(a), it turns out that in the above-threshold regime, $J_c = 0$ around the peak of the number distribution $P_{n,N}$. This is along with Theorem 3. $|J_c|$ further exhibits a Mount-Fuji landscape, in Fig.2(d), revealing a ring ridge that locates an optimal curl flux which reflects the order parameter in Eq.(14). This is expected from Theorems 1 and 3. In the below-threshold regime, however, the curl fluxes diminish. This is a thermal phase in a broader context, as depicted in Fig.2(b). Moreover, in Fig.2(a,c), J_c shows a good agreement with the currents calculated from the graph network approach [63].

Analysis with curl flux network.—Theorem 1 indicates a global nature on the current network [63]. Our hexagonal-grid graph is formed by alternately repeating two elementary triangles ∇, Δ , in an analogy to the tessellation. The network can be reformed into cycle frequency along certain loop trajectories, i.e., $J_{(n,N) \rightarrow (n',N')} = \sum_C (f_{C+} - f_{C-})$ where $f_{C\pm}$ is the cycle frequency along the trajectory C and $J_{(n,N) \rightarrow (n',N')}$ follows Eq.(4) (the summation is over all the trajectories involving the edge $[(n, N) \rightarrow (n', N')]$). The cycle frequency quantifies the number of rounds which the system can transit through a complete cycle per unit time [48, 54, 64, 65]. From the algebraic graph theory, one has the loop affinity $\Phi = \ln(f_{C+}/f_{C-}) = \sum_{i \in \{\text{all } \nabla, \Delta \text{ in loop } C\}} \Phi_i$ along the C , where $\Phi_i = \ln(\Pi_{i+}/\Pi_{i-})$ is the affinity on individual ∇, Δ and $\Pi_{i\pm}$ is a product of the transition rates along individual ∇, Δ on the graph (see Theorem S1 in Ref.[44]). Φ provides a measure of deviation from the equilibrium state, as known from the graph theory.

One further notes from Eq.(2) that $\Pi_{i+}/\Pi_{i-} = \Pi_{\nabla+}/\Pi_{\nabla-}$ is independent of the site index (n, N) and $\Phi_\Delta + \Phi_\nabla = 0$ [44]. Φ_∇, Φ_Δ opposite to each other define the clockwise and counter-clockwise cycles, notable in Fig.3; this generates an edge current on the graph. Using m, n to count the numbers of ∇, Δ inside the loop C , it

TABLE I. Symmetry and topology of the FC/PC, BEC and thermal phases.

	Symmetry	Homotopy	Winding number
FC/PC	\times	\mathbb{Z}	1
Thermal	$U(1)$	\times	0
BEC	\times	\times	0

gives $\Phi = (m - n)\Phi_\nabla$. On the edges, $m - n = I$ ($I \gg 1$ is the edge length) and one finds

$$\Phi = I \cdot \left| \ln \left[\frac{(R+1)S}{R(S+1)} \left(1 + \frac{1}{\bar{n}} \right) \right] \right| \quad (15)$$

which forms a unidirectional edge current, as depicted in Fig. 3.

Eq.(15) shows $\Phi \sim [\text{Perimeter of graph edge}]$, resembling an “area” scaling. Sophistically, Φ —as a difference between forward and backward cycles—can be a topological number for the graph texture.

Discussion and summary.—The FCs have been observed in various materials, where most of the experiments are based on the spectroscopic technique measuring the intensity of emitted photons. Such a conventional optical technique is unable to access neither the counting statistics nor the fluctuations of the excitations, which however play an essential role in understanding the nonequilibrium properties of the FCs. To unveil the information about correlations and fluctuations, new spectroscopic schemes may have to be proposed in the basis of the quantum optical detection. The delayed photon-coincidence counting (DPCC) would be a candidate feasible in the experiments.

The DPCC is performed by placing two photon-number detectors to record the correlation between the emitted photons. The Glauber’s multi-photon coherences are measured, e.g., the g_2 function that may imprint the coherence and fluctuations of molecular excitations. In this vein, the signal $\sim \langle \eta_1^\dagger \eta_1^\dagger(\tau) \eta_1(\tau) \eta_1 \rangle$, the prefactor arising from the temporal gate parameters in detectors. It is anticipated that the FC phase may lead to oscillations in the time-resolved signals. This is consistent with the cycling nature of curl fluxes that is likely to be coherent. In the infrared regime, the DPCC measurement requires the time gates with a duration ~ 1 ps which is achievable in laboratories.

Next let us look into the experimental feasibility of achieving the FC phase in infrared regime. For a generic estimation, taking $R = S$ would be reasonable so that the threshold is $R_c \approx \bar{n} + \frac{1}{M\alpha} + \frac{1}{M}$. For organic molecules, the vibrational decay $\gamma^{-1} \sim 100$ ps. Using $M = 100$, $\alpha \sim 0.07$, $\bar{n} \sim 3$ (ambient temperature), one has the energy pump to create the FCs $p = 10MR_c\gamma\hbar\omega_\nabla \sim 7.2 \times 10^{-7}$ W. With the area $A \sim 1$ mm² of NIR laser spot shining on the sample and the cross section of light scattering

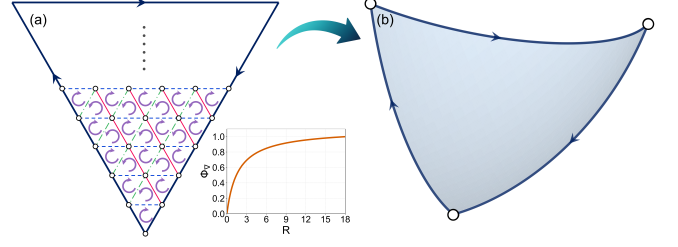


FIG. 3. Illustration of the loop affinity. (a) Loop affinities for ∇, Δ such that $\Phi_\Delta = -\Phi_\nabla$ indicate opposite cycles (purple arrows). An edge current is presented thereby (big arrows). Small panel: loop affinity vs. pump rate. (b) Loop affinity in Eq.(15) as a topological quantity, regardless of deformations of the graph.

for resonance absorption at near-infrared wavelength $\sigma \sim 10^{-8}$ cm², the number of photons needed for a considerable capture is $N = A/\sigma \sim 10^6$. Therefore the pump power is estimated to be $P = Np/\phi \sim 1$ W, given the pump efficiency $\phi = 70\%$.

In summary, our work presents a thorough study of the nonequilibrium condensate of bosons, in conjunction with the Fröhlich condensation. Our quantum theory elucidated the detailed-balance-breaking nature through the curl flux network, revealing topological variation when driven far from equilibrium. A generic order parameter was identified for the Fröhlich condensation, showing graph texture beyond the symmetry-breaking paradigm of phase transitions. The results clearly demonstrated, on the graphs of the curl flux network, that the PCs rest in the regime of Fröhlich condensation. Understanding the nonequilibrium phases of matter will enrich the studies of complex systems coupled to external fields, thereby significantly advancing the frontier of the statistical thermodynamics at mesoscopic scale.

Remarks.—It is worth noting from our model that the loop affinities associated with Δ, ∇ are opposite. This means the graph texture with the PCs differs from the topological edge chiral modes that have been explored in electronic materials [66, 67]. Nevertheless, the nonlocal curl flux emerges from the probability edge currents [i.e., Eq.(4)] that may generate optimal loops—as proven in $J_c(z, z^*)$ exhibiting the Mount-Fuji landscape—which possess the topology of the graph. Such a topological structure therefore dictates a dynamics distinct from the topology-protected chiral edge states.

F. L. and C. S. contributed equally to this work.

We thank Sam Sung Ching Wong from City University of Hong Kong for the instructive discussions. Z.D.Z. and F. L. gratefully acknowledge the support of the Excellent Young Scientists Fund by National Science Foundation of China (No. 9240172), the General Fund by National Science Foundation of China (No. 12474364), and the National Science Foundation of China/RGC

Collaborative Research Scheme (No. 9054901). Z. L. and C. S. gratefully acknowledge the support of the National Science Foundation (No. DMR-2145256).

* zhiyuelu@unc.edu

† zzhan26@cityu.edu.hk

- [1] E. Perez-Martin, T. Beranger, L. Bonnet, F. Teppe, A. Lisauskas, *et al.*, *Sci. Adv.* **11**, eadv0346 (2025)
- [2] A. V. Zasedatelev, A. V. Baranikov, D. Urbonas, F. Scafrimuto, U. Scherf, T. Stöferle, R. F. Mahrt and P. G. Lagoudakis, *Nat. Photonics* **13**, 378-383 (2019)
- [3] W. Xu, A. A. Bagrov, F. T. Chowdhury, L. D. Smith, D. R. Kattnig, H. J. Kappen and M. I. Katsnelson, *Phys. Rev. Research* **7**, 023111-023123 (2025)
- [4] A. Amo, D. Sanvitto, F. P. Laussy, D. Ballarini, E. del Valle *et al.*, *Nature* **457**, 291-295 (2009)
- [5] W. Xiong, *Acc. Chem. Res.* **56**, 776-786 (2023)
- [6] J. T. Mäkinen, S. Autti and V. B. Eltsov, *Appl. Phys. Lett.* **124**, 100502-100515 (2024)
- [7] J. Sheng, J.-W. Mei, L. Wang, X. Xu, W. Jiang, *et al.*, *Nat. Mater.* **24**, 544-551 (2025)
- [8] H. Fröhlich, *Int. J. Quantum Chem.* **2**, 641-649 (1968)
- [9] J. Preto, *J. Bio. Phys.* **43**, 167-184 (2017)
- [10] T. M. Wu and S. Austin, *J. Theor. Bio.* **71**, 209-214 (1978)
- [11] I. V. Lundholm, H. Rodilla, W. Y. Wahlgren, A. Duelli, G. Bourenkov, *et al.*, *Struct. Dyn.* **2**, 054702-054713 (2015)
- [12] A. Chandran, T. Iadecola, V. Khemani and R. Moessner, *Ann. Rev. Condens. Matter Phys.* **14**, 443-469 (2022)
- [13] Z. Ge, A. M. Graf, J. Keski-Rahkonen, S. Slizovskiy, P. Polizogopoulos, *et al.*, *Nature* **635**, 841-846 (2024)
- [14] J. Song, S. Ghosh, X. Deng, C. Li, Q. Shang, *et al.*, *Sci. Adv.* **11**, eadr1652 (2025)
- [15] C. Schneider, A. Rahimi-Iman, N. Y. Kim, J. Fischer, I. G. Savenko, *et al.*, *Nature* **497**, 348-352 (2013)
- [16] M. Kowalewski, K. Bennett and S. Mukamel, *J. Phys. Chem. Lett.* **7**, 2050-2054 (2016)
- [17] J. Galego, F. J. Garcia-Vidal and J. Feist, *Nat. Commun.* **7**, 13841-13846 (2016)
- [18] J. R. Reimers, L. K. McKemmish, R. H. McKenzie, A. E. Mark and N. S. Hush, *PNAS* **106**, 4219-4224 (2009)
- [19] Z. D. Zhang, G. S. Agarwal and M. O. Scully, *Phys. Rev. Lett.* **122**, 158101-158106 (2019)
- [20] J. Kasprzak, M. Richard, S. Kundermann, A. Baas, P. Jeambrun, *et al.*, *Nature* **443**, 409-414 (2006)
- [21] R. Su, A. Fieramosca, Q. Zhang, H. S. Nguyen, E. Deleporte, Z. Chen, D. Sanvitto, T. C. H. Liew and Q. Xiong, *Nat. Mater.* **20**, 1315-1324 (2021)
- [22] Y. Sun, P. Wen, Y. Yoon, G. Liu, M. Steger, L. N. Pfeiffer, K. West, D. W. Snoke and K. A. Nelson, *Phys. Rev. Lett.* **118**, 016602-016607 (2017)
- [23] T. M. Wu and S. J. Austin, *J. Bio. Phys.* **9**, 97-107 (1981)
- [24] I. Nardecchia, J. Torres, M. Lechelon, V. Giliberti, M. Ortolani, *et al.*, *Phys. Rev. X* **8**, 031061-031083 (2018)
- [25] R. Su, S. Ghosh, J. Wang, S. Liu, C. Diederichs, T. C. H. Liew and Q. Xiong, *Nat. Phys.* **16**, 301-306 (2020)
- [26] H. Deng, G. Weihs, C. Santori, J. Bloch and Y. Yamamoto, *Science* **298**, 199-202 (2002)
- [27] M. Struve, C. Bennenhei, H. P. Adl, K. W. Song, H. Shan, *et al.*, arXiv:2408.13677
- [28] J. D. Plumhof, T. Stöferle, L. Mai, U. Scherf and R. F. Mahrt, *Nat. Mater.* **13**, 247-252 (2014)
- [29] H. Deng, H. Haug and Y. Yamamoto, *Rev. Mod. Phys.* **82**, 1489-1537 (2010)
- [30] T. Byrnes, N. Y. Kim and Y. Yamamoto, *Nat. Phys.* **10**, 803-813 (2014)
- [31] L. V. Butov, *Nature* **447**, 540-541 (2007)
- [32] L. V. Butov and A. V. Kavokin, *Nat. Photonics* **6**, 2 (2012)
- [33] B. Deveaud-Pledran, *Nat. Photonics* **6**, 205 (2012)
- [34] G. Lerario, A. Fieramosca, F. Barachati, D. Ballarini, K. S. Daskalakis, *Nat. Phys.* **13**, 837-841 (2017)
- [35] X. Chen, H. Alnatah, D. Mao, M. Xu, Y. Fan, *et al.*, *Nano Lett.* **23**, 9538-9546 (2023)
- [36] E. Estrecho, T. Gao, N. Bobrovska, M. D. Fraser, M. Steger, *et al.*, *Nat. Commun.* **9**, 2944-2952 (2018)
- [37] M. Pieczarka, E. Estrecho, M. Boozarjimehr, O. Bleu, M. Steger, *et al.*, *Nat. Commun.* **11**, 429-435 (2020)
- [38] P. Schwendimann and A. Quattropani, *Phys. Rev. B* **77**, 085317-085329 (2008)
- [39] Z. D. Zhang, S. Zhao and D. Lei, *Phys. Rev. B* **106**, L220306-L220313 (2022)
- [40] X. Wang and J. Wang, *Phys. Rev. B* **106**, L220103-L220109 (2022)
- [41] M. Klaas, E. Schlottmann, H. Flayac, F. P. Laussy, F. Gericke, *et al.*, *Phys. Rev. Lett.* **121**, 047401- 047406 (2018)
- [42] F. P. Laussy, G. Malpuech, A. Kavokin and P. Bigenwald, *Phys. Rev. Lett.* **93**, 016402-016405 (2004)
- [43] G. Sethi, M. Cuma and F. Liu, *Phys. Rev. Lett.* **130**, 186401-186407 (2023)
- [44] See Supplemental Material at ... for a detailed description of the quantum theory of nonequilibrium bosons.
- [45] The equation of motion for the off-diagonal elements will be presented elsewhere.
- [46] T. L. Hill and O. Kedem, *J. Theor. Biol.* **10**, 399-441 (1966)
- [47] T. L. Hill and Y.-D. Chen, *Proc. Natl. Acad. Sci. U.S.A.* **72**, 1291-1295 (1975)
- [48] J. Schnakenberg, *Rev. Mod. Phys.* **48**, 571-585 (1976)
- [49] J. Wang, *Adv. Phys.* **64**, 1-137 (2015)
- [50] J. Wang, L. Xu and E. Wang, *PNAS* **105**, 12271-12276 (2008)
- [51] H. Qian, *Ann. Rev. Phys. Chem.* **58**, 113-142 (2007)
- [52] Z. D. Zhang and J. Wang, *J. Chem. Phys.* **140**, 245101-245114 (2014)
- [53] Z. D. Zhang and J. Wang, *New J. Phys.* **17**, 043053-043073 (2015)
- [54] L. Wang, Z. Wang, C. Wang and J. Ren, *Phys. Rev. Lett.* **128**, 067701-067706 (2022)
- [55] M. O. Scully, *Phys. Rev. Lett.* **82**, 3927-3930 (1999)
- [56] C. N. Yang, *Rev. Mod. Phys.* **34**, 694-704 (1962)
- [57] A. J. Leggett, *Rev. Mod. Phys.* **73**, 307-356 (2001)
- [58] V. V. Albert and L. Jiang, *Phys. Rev. A* **89**, 022118-022131 (2014)
- [59] L. M. Sieberer, M. Buchhold and S. Diehl, *Rep. Prog. Phys.* **79**, 096001-096068 (2016)

[60] The \mathbf{F} and \mathbf{D} matrices are of the form

$$\mathbf{F} = - \begin{pmatrix} \frac{1}{2} \left[x - \frac{R}{V} + S \frac{A}{V} - (S+1) \frac{B}{V} \right] - \alpha' \left[\left(x + \frac{1}{V} \right) \frac{K}{V} - x \frac{H}{V} \right] \\ \frac{\sqrt{3}}{2} \left[x - \frac{R}{V} - S \frac{A}{V} + (S+1) \frac{B}{V} \right] \end{pmatrix} \quad (16a)$$

$$\mathbf{D} = \frac{1}{8V} \begin{pmatrix} [r(x) + p] + 4\alpha' \left[x \frac{K}{V} + \left(x + \frac{1}{V} \right) \frac{H}{V} \right] & \sqrt{3} [r(x) - p] \\ \sqrt{3} [r(x) - p] & 3 [r(x) + p] \end{pmatrix} \quad (16b)$$

with $\alpha' = \alpha V$, $r(x) = (2R+1) \left(X + \frac{Y}{\sqrt{3}} \right) + \frac{R+1}{V}$, $p = S \frac{A}{V} + (S+1) \frac{B}{V}$.

[61] The space of circles is isomorphic to the Abelian group, as seen from the product operation $\phi_2 \cdot \phi_1$ that is commutative. $e^{in\theta}$ forms an irreducible representation of the Abelian group where the integer n counts the number of rounds for a periodic boundary condition.

- [62] V. Y. Shishkov, E. S. Andrianov, A. V. Zasedatelev, P. G. Lagoudakis and Lozovik, Phys. Rev. Lett. **128**, 065301-065306 (2022).
- [63] Noting the divergence-free nature from Eq.(2), the current network can be decomposed into a series of closed loops. To confirm this, we calculate in hexagonal-grid graph the net edge currents associated with site (n, N) , and plot in Fig.2(d). The cycle flux around $P_{n,N}$'s peak is observed, when above the pump threshold. This implies a graph topology corresponding to a winding number $Q = 1$, in a consistency with the results from the continuous limit.
- [64] T. L. Hill, *Introduction to Irreversible Thermodynamics*
- [65] M. Polettini and M. Esposito, J. Stat. Mech. (2014) P10033
- [66] X. L. Qi and S.-C. Zhang, Rev. Mod. Phys. **83**, 1057-1110 (2011)
- [67] E. Tang, J. Agudo-Canalejo and R. Golestanian, Phys. Rev. X **11**, 031015-031034 (2021)